Electron specific absorbed fractions for the adult male and female ICRP/ICRU reference computational phantoms

Maria Zankl, Helmut Schlattl, Nina Petoussi-Henss, Christoph Hoeschen

Research Unit Medical Radiation Physics and Diagnostics, Helmholtz Zentrum München – German Research Center for Environmental Health, Ingolstädter Landstr. 1, 85764 Neuherberg, Germany

E-mail: zankl@helmholtz-muenchen.de

Short title: Electron SAFs for the adult male and female

PACS numbers: 87.53.Bn, 87.57.uq, 87.57.uk

Keywords: Specific absorbed fraction, electron, reference computational phantoms, self-absorption, cross-fire, reciprocity

Abstract

The calculation of radiation dose from internally incorporated radionuclides is based on so-called absorbed fractions (AF) and specific absorbed fractions (SAF). Specific absorbed fractions for monoenergetic electrons were calculated for 63 source regions and 67 target regions using the new male and female adult reference computational phantoms adopted by the ICRP and ICRU and the Monte Carlo radiation transport programme package EGSnrc. The SAF values for electrons are opposed to the simplifying assumptions of ICRP Publication 30. The previously applied assumption of electrons being fully absorbed in the source organ itself is not always true at electron energies above approximately 300-500 keV. High-energy electrons have the ability to leave the source organ and, consequently, the electron SAFs for neighbouring organs can reach the same magnitude as those for photons for electron energies above 1 MeV. The reciprocity principle known for photons can be extended to electron SAFs as well, thus making cross-fire electron SAFs mass-independent. To quantify the impact of the improved electron dosimetry in comparison to the dosimetry using the simple assumptions of ICRP Publication 30, absorbed doses per administered activity of three radiopharmaceuticals were evaluated with and without explicit electron transport. The organ absorbed doses per administered activity for the two evaluation methods agree within 2-3% for most organs for radionuclides with decay spectra having electron energies below a few hundred keV and within approximately 20% if higher electron energies are involved. An important exception is the urinary bladder wall, where the dose is overestimated by between 60% and 150% by the simplified ICRP 30 approach for the radiopharmaceuticals of this study.

Introduction

The calculation of radiation dose from internally incorporated radionuclides is based on absorbed fractions (AFs) that specify the fraction of energy emitted by radioactivity in a given source region which is absorbed in that region itself and in other target regions (Loevinger *et*

al 1988). The absorbed fraction divided by the mass of the target region is called the specific absorbed fraction, SAF.

Until recently, photon SAFs were calculated using MIRD-type mathematical anthropomorphic phantoms at various ages (Cristy and Eckerman 1987a, b, c, d, e, f, g, Cristy and Eckerman 1993). A new generation of phantoms, based on medical image data of real persons, are now used for internal dosimetry and could significantly contribute to better dose assessment (Guo *et al* 2010, Kramer *et al* 2010, Stabin *et al* 2012, Wayson *et al* 2012). The ICRP (International Commission on Radiological Protection) and ICRU (International Commission on Radiation Units and Measurements) have adopted reference computational phantoms (ICRP 2009) representing the Reference Male and Reference Female (ICRP 2002, 2007) for their ongoing revision of calculated dose coefficients following the recent ICRP Recommendations (ICRP 2007). This will include, among others, specific absorbed fractions for electrons, photons, neutrons and alpha particles.

For electrons, SAF values stemming from particle transport calculations are available only for specific source/target region combinations in the human respiratory tract (ICRP 1994), the human alimentary tract (ICRP 2006), and the skeleton (ICRP 1979), which have been evaluated using specifically designed stylised anatomical models. For all other source/target region combinations, the following approximations were used (ICRP 1979):

$$\phi(r_T \leftarrow r_S) = \begin{cases} 1 & \text{for } r_T = r_S \\ 0 & \text{for } r_T \neq r_S \\ 0.5\, M_w / M_c & \text{for } r_T = \text{wall}, r_S = \text{contents of walled organ} \\ M_T / M_{TB} & \text{for } r_S = \text{Total body} \end{cases} \quad (1)$$

where r_S is the source region, r_T is the target region, $\phi(r_T \leftarrow r_S)$ is the fraction of energy emitted in r_S that is absorbed in r_T (AF), M_w and M_c are the masses of the wall and the contents of a walled organ, respectively, TB is the total body, and M_T and M_{TB} are the masses of the target region and the total body, respectively. Note that in internal dosimetry, the term "total body" means only the biological tissues of the body and excludes the contents of walled organs in the alimentary, urinary and respiratory tracts.

These approximations for the absorbed fractions result in the following specific absorbed fractions:

$$\Phi(r_T \leftarrow r_S) = \begin{cases} 1/M_T & \text{for } r_T = r_S \\ 0 & \text{for } r_T \neq r_S \\ 0.5/M_c & \text{for } r_T = \text{wall}, r_S = \text{contents of walled organ} \\ 1/M_{TB} & \text{for } r_S = \text{Total body} \end{cases} \quad (2)$$

With the contemporary availability of powerful computers and radiation transport programmes that enable detailed simulation of electron transport, Monte Carlo calculations of electron SAFs have become feasible. Hence, there is no necessity any more to rely on the above approximations. It has already been shown earlier that the assumption of electrons being fully absorbed in the source organ itself is not always true at higher energies (Chao and Xu 2001). Therefore, the ICRP has decided to incorporate Monte Carlo calculated electron SAFs for the organ dose coefficients in its forthcoming publications on occupational intakes of radionuclides and on nuclear medical applications of radiopharmaceuticals. Preliminary photon and electron SAF data for selected source and target regions have been shown in

graphical form in ICRP Publication 110 (ICRP 2009) and were further presented by Hadid *et al* (2010), where also the numerical data have been included.

The reference computational phantoms have been used to calculate a large set of SAFs for monoenergetic electrons, encompassing 61 source and 68 target regions. The present work summarises these data, reveals improvements compared to the above approximations, and discusses some general features of electron SAFs, such as mass dependence and reciprocity. Furthermore, the possibility is examined to complement the specific respiratory tract (ICRP 1994), alimentary tract (ICRP 2006) and skeleton (Hough *et al* 2011, ICRP 1979) electron SAFs with the SAF values calculated in the reference computational phantoms.

The numerical electron SAF data for all source and target region combinations as calculated using the reference computational phantoms are given as online supplementary data. These data will be the basis for the electron SAFs to be presented in a forthcoming ICRP publication (ICRP in preparation).

Materials and Methods

Monte Carlo code

The electron transport was simulated with EGSnrc Version V4-2-2-5 (Kawrakow *et al* 2009, Kawrakow and Rogers 2003) using a Class II condensed history technique (Berger 1963), which transports secondary particles produced above a certain chosen energy. Bremsstrahlung cross sections for kinetic energies below 1 GeV agree with those of the NIST database (Seltzer and Berger 1985, Seltzer and Berger 1986), which in turn form the basis for the radiative stopping powers recommended by ICRU (ICRU 1984). At the energies relevant for this study, electron impact ionisation was modelled using default cross sections (Kawrakow 2002). A revised transport algorithm for multiple scattering has been implemented in EGSnrc (Kawrakow and Bielajew 1998), which allows larger transport steps than in EGS4 (Nelson *et al* 1985). For elastic scattering, spin effects are taken into account. Pair production is simulated in the same way as in EGS4 (Nelson *et al* 1985). Triplet-production processes are neglected for all particles. The cutoff energy for electrons with an initial kinetic energy below 50 keV was 2 keV and 20 keV otherwise. Electrons with kinetic energies below 500 keV rarely reach distant target regions. The energy absorbed in those organs is low and mainly caused by bremsstrahlung production within the source region. To decrease the relative statistical uncertainty in the SAFs of distant target regions, a variance reduction technique called bremsstrahlung splitting was employed (Kawrakow *et al* 2009).

The ICRP/ICRU adult reference computational phantoms

For the computations of organ absorbed fractions and specific absorbed fractions, the adult male and female reference computational phantoms, representing the ICRP/ICRU adult Reference Male and Reference Female (ICRP 2007) were used for this study. These phantoms were adopted by the ICRP and ICRU as the official phantoms for the computation of the ICRP/ICRU reference dose coefficients and are extensively described in ICRP Publication 110 (ICRP 2009). The reference computational models are digital three-dimensional representations of human anatomy and are based on computed tomographic data of real people. They are largely consistent with the information given in ICRP Publication 89 (ICRP 2002) on the reference anatomical parameters for both male and female adults. The reference computational phantoms were constructed by modifying the voxel models Golem (Zankl and Wittmann 2001) and Laura (Zankl *et al* 2005) of two individuals whose body height and mass closely resembled the reference data. Most organ masses of both phantoms were adjusted to

the ICRP data on the Reference Male and Reference Female with high precision, without significantly altering their realistic anatomy. The phantoms contain all target regions relevant to the assessment of human exposure to ionising radiation for radiological protection purposes, i.e. all organs and tissues that contribute to the quantity effective dose (ICRP 2007). For the sake of brevity, these phantoms will also be called "RCP-AM" (Reference Computational Phantom – Adult Male) and "RCP-AF" (Reference Computational Phantom – Adult Female) in the following.

Both phantoms are represented in the form of three dimensional arrays of cuboid voxels (= volume elements), and the voxels are arranged in columns, rows and slices. Each entry in the array identifies the organ or tissue to which the corresponding voxel belongs. The RCP-AM consists of approximately 1.95 million tissue voxels (excluding voxels representing the surrounding vacuum) each with a slice thickness (corresponding to the voxel height) of 8.0 mm and an in-plane resolution (i.e., voxel width times depth) of 2.137×2.137 mm², corresponding to a voxel volume of 36.54 mm^3. The number of slices is 220, resulting in a body height of 1.76 m; the body mass is 73 kg. The RCP-AF consists of approximately 3.89 million tissue voxels, each with a slice thickness of 4.84 mm and an in-plane resolution of 1.775×1.775 mm^2, corresponding to a voxel volume of 15.25 mm^3. The number of slices is 346, and the body height is 1.63 m; the body mass is 60 kg. The number of individually segmented structures is 136 in each phantom, and fifty-three different tissue compositions have been assigned to them. The various tissue compositions account for both the elemental composition of the tissue parenchyma (ICRU 1992) and each organ's blood content (ICRP 2002). Figure 1 shows frontal (coronal) views of the RCP-AM (left) and RCP-AF (right), respectively.

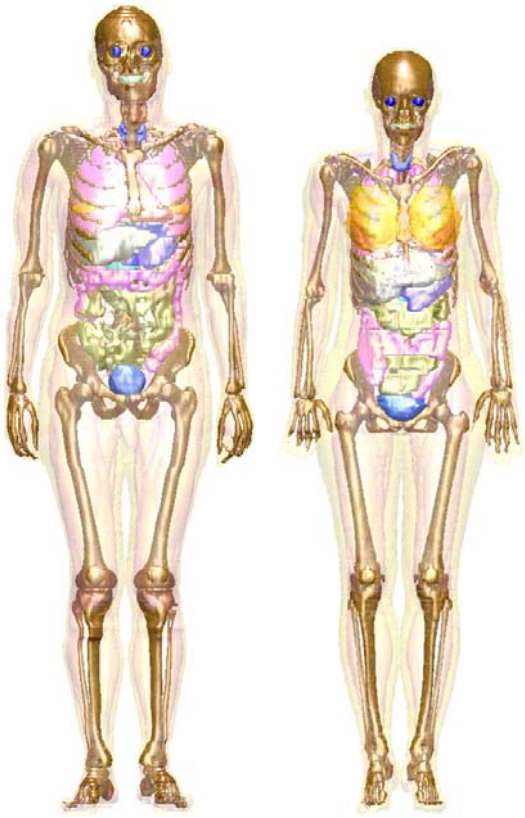

Figure 1. Images of the male (left) and female (right) computational phantoms. The following organs can be identified by different surface colours: breast, bones, colon, eyes, lungs, liver, pancreas, small intestine, stomach, teeth, thyroid and urinary bladder. Muscle and adipose tissue are displayed as transparent. For illustration purposes, the voxelised surfaces have been smoothed.

Source and target regions

As described above, the resolution of the tomographic data on which these phantoms are based is limited; on the other hand some of the source and target regions have very small dimensions. Hence, not all tissues could be explicitly represented. In the skeleton, for example, the target regions of interest are the red bone marrow in the marrow cavities of spongiosa and the endosteal layer lining these cavities (presently assumed to be 50 μm in thickness). The endosteal tissue is also termed as "shallow marrow" or, in former ICRP terminology, as "bone surface". Due to their small dimensions, these two target regions had to be incorporated as constituents of homogeneous spongiosa volumes within the reference phantoms. At lower energies of photons (and neutrons), secondary charged-particle equilibrium is not fully established in these tissue regions over certain energy ranges. More refined techniques for accounting for these effects in skeletal dosimetry have been developed at the University of Florida (Hough *et al* 2011, ICRP 2010, Johnson *et al* 2011, Jokisch *et al* 2011a, Jokisch *et al* 2011b) and by Kramer *et al* (2011). For the present work, the electron SAFs to red bone marrow and endosteum as targets from source regions outside the skeleton have been evaluated as mass-weighted sum of the SAFs to the homogeneous spongiosa regions of the individual bones as follows:

$$\Phi(R\text{-}marrow \leftarrow r_S) = \sum_T \frac{M_{\text{R-marrow,T}}}{M_{\text{R-marrow}}} \Phi(Spongiosa, T \leftarrow r_S) \quad (3)$$

and

$$\Phi(Endost-BS \leftarrow r_S) = \sum_T \frac{M_{\text{Endost-BS,T}}}{M_{\text{Endost-BS}}} \Phi(Spongiosa, T \leftarrow r_S)$$

where $M_{\text{R-marrow,T}}$ is the mass of red bone marrow in bone T, $M_{\text{R-marrow}}$ is the mass of the red bone marrow in the whole skeleton, $M_{\text{Endost-BS,T}}$ is the endosteal tissue in bone T, $M_{\text{Endost-BS}}$ is the mass of the endosteal tissue in the whole skeleton, and $\Phi(Spongiosa, T \leftarrow r_S)$ is the specific absorbed fraction to the spongiosa of bone T from source region r_S. Specific absorbed fractions to the skeletal target regions from sources inside the skeleton have not been considered in this work.

Further target regions whose resolutions are finer than the voxel resolutions of the reference computational phantoms are located in the alimentary and respiratory tracts. For these tissues, the ICRP no longer considers the mean absorbed dose in the entire organ to be the dose quantity of relevance, but rather the absorbed dose to the stem cells or cells at risk. Detailed calculations of absorbed fractions to the stem cells in the walls of the alimentary tract organs from sources in the contents and in the walls of these organs have been performed with stylised models and have been presented in ICRP Publication 100 (ICRP 2006). Similarly, absorbed fractions of energy for various stem cell populations in the respiratory tract from sources in the airway regions have been simulated separately and have been presented in ICRP Publication 66 (ICRP 1994). Since these source and target regions cannot be represented at their true resolution in the reference computational phantoms, no attempt has been made to re-evaluate these specific absorbed fractions. However, the findings of the present work suggest that electron SAFs for cross-fire between regions inside and outside the alimentary and respiratory tracts can be evaluated with the reference computational phantoms, as will be discussed below. For this purpose, those high-resolution source and target regions were represented by "surrogate" regions that have approximately the same anatomical position, albeit their anatomical realism is limited by the coarser resolution of the Reference Computational Phantoms.

The source regions of this work are listed in Table 1 together with their acronyms as introduced in ICRP Publication 110 (ICRP 2009), the target regions are listed in Table 2. In

case surrogate regions have been used for evaluation cross-fire SAFs from a source region or to a target region, these surrogate regions are given as well in these tables.

Table 1. List of all source regions used for the calculations of this work. The acronyms denoting these source regions in the accompanying electronic files are given as well. The acronyms are those introduced in ICRP Publication 110 (ICRP 2009). For the source regions marked with an asterisk, only cross-fire SAFs to target regions other than the source region (or its wall, in case of source regions in the contents of a walled organ) are considered in this work. For some source regions that could not be represented at their true resolution, so-called "surrogate" regions have been used. These are indicated in a separate column.

	Source region	Acronym	Surrogate region
*	Oral cavity	O-cavity	Oral mucosa
	Oral mucosa	O-mucosa	
	Teeth surface activity	Teeth-S	Teeth volume activity
	Teeth volume activity	Teeth-V	
	Tongue	Tongue	
	Tonsils	Tonsils	
*	Oesophagus fast	Oesophag-f	Oesophagus
*	Oesophagus slow	Oesophag-s	Oesophagus
*	Oesophagus wall	Oesophagus	
*	Stomach contents	St-cont	
*	Stomach wall	St-wall	
*	Small intestine contents	SI-cont	
*	Small intestine wall	SI-wall	
*	Small intestine villi	SI-villi	Small intestine wall
*	Right colon contents	RC-cont	
*	Right colon wall	RC-wall	
*	Left colon contents	LC-cont	
*	Left colon wall	LC-wall	
*	Recto-sigmoid colon contents	RSig-cont	
*	Recto-sigmoid colon wall	RSig-wall	
*	Surface of anterior nasal passages	ET1-sur	ET_1
*	Surface of posterior nasal passages + pharynx	ET2-sur	ET_2
*	Bound ET_2 region	ET2-bnd	ET_2
*	Sequestered ET_2 region	ET2-seq	ET_2
	Lymph nodes in extrathoracic (ET) region	LN-ET	
*	Bronchi	Bronchi	
*	Bronchi bound	Bronchi-b	Bronchi
*	Bronchi sequestered	Bronchi-s	Bronchi
*	Bronchioles	Bronchiole	
*	Bronchioles bound	Brchiole-b	Bronchiole
*	Bronchioles sequestered	Brchiole-q	Bronchiole
	Alveolar-interstitium	AI	Lung tissue
	Lymph nodes in thoracic region	LN-Th	
	Lungs	Lungs	
	Adrenals	Adrenals	
	Blood in heart	Ht-cont	
	Blood vessels of head, trunk, arms, legs, left and right lungs, and blood in organs	Blood	
*	Cortical bone mineral surface	C-bone-S	Cortical bone mineral volume
*	Cortical bone mineral volume	C-bone-V	
*	Trabecular bone mineral surface	T-bone-S	Trabecular bone mineral volume
*	Trabecular bone mineral volume	T-bone-V	Mineral bone fraction of spongiosa
*	Cortical bone marrow	C-marrow	
*	Trabecular bone marrow	T-marrow	Marrow fraction of spongiosa
*	Red (active) bone marrow	R-marrow	Red marrow fraction of spongiosa

*	Yellow (inactive) bone marrow	Y-marrow	Yellow marrow fraction of spongiosa + medullary cavities
	Brain	Brain	
	Breast adipose tissue	Breast-a	
	Breast glandular tissue	Breast-g	
	Breast	Breast	
	Eye lenses	Eye-lens	
	Gall bladder wall	GB-wall	
	Gall bladder contents	GB-cont	
	Heart wall	Ht-wall	
	Kidneys	Kidneys	
	Liver	Liver	
	Lymph nodes, except LN-ET + LN-Th	Lymph	
	Muscle	Muscle	
	Ovaries	Ovaries	
	Pancreas	Pancreas	
	Pituitary gland	P-gland	
	Prostate	Prostate	
	Salivary glands	S-glands	
	Skin	Skin	
	Spinal cord	Sp-cord	
	Spleen	Spleen	
	Testes	Testes	
	Thymus	Thymus	
	Thyroid	Thyroid	
	Ureters	Ureters	
	Urinary bladder wall	UB-wall	
	Urinary bladder contents	UB-cont	
	Uterus/cervix	Uterus	
	Adipose/residual tissue	Adipose	
	Total body tissues (total body minus contents of walled organs)	T-body	
	Soft tissue (Total body tissues minus mineral bone)	S-tissue	

Table 2. List of all target regions used for the calculations of this work. The acronyms denoting these target regions in the accompanying electronic files are given as well. The acronyms are those introduced in ICRP Publication 110 (ICRP 2009). For the target regions marked with an asterisk, only cross-fire SAFs from source regions other than the target region (or its contents, in case of walled organs) are considered in this work.

	Target region	Acronym	Surrogate region
*	Red (active) bone marrow	R-marrow	Spongiosa regions (mass weighted)
	Colon	Colon	
	Lungs	Lungs	
*	Stomach wall	St-wall	
	Breast	Breast	
	Ovaries	Ovaries	
	Testes	Testes	
	Urinary bladder wall	UB-wall	
*	Oesophagus wall	Oesophagus	Oesophagus
	Liver	Liver	
	Thyroid	Thyroid	
*	50-μm endosteal region	Endost-BS	Spongiosa regions (mass weighted)
	Brain	Brain	
	Salivary glands	S-glands	
	Skin	Skin	
	Adrenals	Adrenals	
	Extrathoracic region	ET	

	Gall bladder wall	GB-wall	
	Heart wall	Ht-wall	
	Kidneys	Kidneys	
	Lymph nodes, except LN-ET + LN-Th	Lymph	
	Muscle	Muscle	
*	Oral mucosa	O-mucosa	
	Pancreas	Pancreas	
	Prostate	Prostate	
*	Small intestine wall	SI-wall	
	Spleen	Spleen	
	Thymus	Thymus	
	Uterus/cervix	Uterus	
	Tongue	Tongue	
	Tonsils	Tonsils	
*	Right colon wall	RC-wall	
*	Left colon wall	LC-wall	
*	Recto-sigmoid colon wall	RSig-wall	
*	Basal cells of anterior nasal passages	ET1-bas	ET_1
*	Basal cells of posterior nasal passages + pharynx	ET2-bas	ET_2
	Lymph nodes in extrathoracic (ET) region	LN-ET	
*	Basal cells of bronchi	Bronch-bas	Bronchi
*	Secretory cells of bronchi	Bronch-sec	Bronchi
*	Secretory cells of bronchioles	Bchiol-sec	Lung tissue
	Alveolar-interstitium	AI	Lung tissue
	Lymph nodes in thoracic region	LN-Th	
	Right lung lobe	RLung	
	Left lung lobe	LLung	
	Right adrenal gland	RAdrenal	
	Left adrenal gland	LAdrenal	
	Right breast adipose tissue	RBreast-a	
	Right breast glandular tissue	RBreast-g	
	Left breast adipose tissue	LBreast-a	
	Left breast glandular tissue	LBreast-g	
	Right breast	RBreast	
	Left breast	LBreast	
	Breast adipose tissue	Breast-a	
	Breast glandular tissue	Breast-g	
	Eye lenses	Eye-lens	
	Right kidney cortex	RKidney-C	
	Right kidney medulla	RKidney-M	
	Right kidney pelvis	RKidney-P	
	Right kidney	RKidney	
	Left kidney cortex	LKidney-C	
	Left kidney medulla	LKidney-M	
	Left kidney pelvis	LKidney-P	
	Left kidney	LKidney	
	Right ovary	ROvary	
	Left ovary	LOvary	
	Pituitary gland	P-gland	
	Spinal cord	Sp-cord	
	Ureters	Ureters	
	Adipose/residual tissue	Adipose	

Calculations performed

Homogeneous volume sources of monoenergetic electrons were simulated in each of the source regions of Table 1. Twenty-five electron energies ranging from 10 keV to 10 MeV were considered. Note that with "electron energy" here and in the following always the kinetic electron energy is meant. Per electron energy and source region, ten million electron histories were followed. The resulting statistical uncertainties show a large variability and

depend significantly on the respective absorbed fractions. For distant organ pairs where only a very small proportion of the energy released in the source organ can reach the target organ, the statistical uncertainties are quite high; on the other hand, in these cases the absorbed fractions and specific absorbed fractions are quite small, and thus large uncertainties appear acceptable. The overall average of the coefficients of variance for all 168354 non-zero AF values of this study is 11.84%, with approximately 70% of these AF being below 0.0001. For AF between 0.0001 and 0.001, the coefficients of variance are on average 1.24%; for AF between 0.001 and 0.01, the coefficients of variance are on average 0.56%; for an AF range between 0.01 and 0.1, this average is 0.24%; and for AF between 0.1 and 1, the average of the coefficients of variance is 0.08%.

To examine the practical relevance of the electron transport calculations, two sets of absorbed doses per administered activity for selected radiopharmaceuticals have been evaluated, one using the electron SAFs of this work, the other with the approximations of equation (2).

Results and Discussion

1. *Assumption* $\Phi(r_S \leftarrow r_S) = 1/M_S$ *for absorption in the source region itself*

Since the beta rays released by the nuclear transformations of most radionuclides have only low penetrability and do not travel far in human tissues, equation (1) assumes complete local electron absorption in the source organ resulting in an energy-independent SAF value corresponding to the inverse of the source/target region mass.

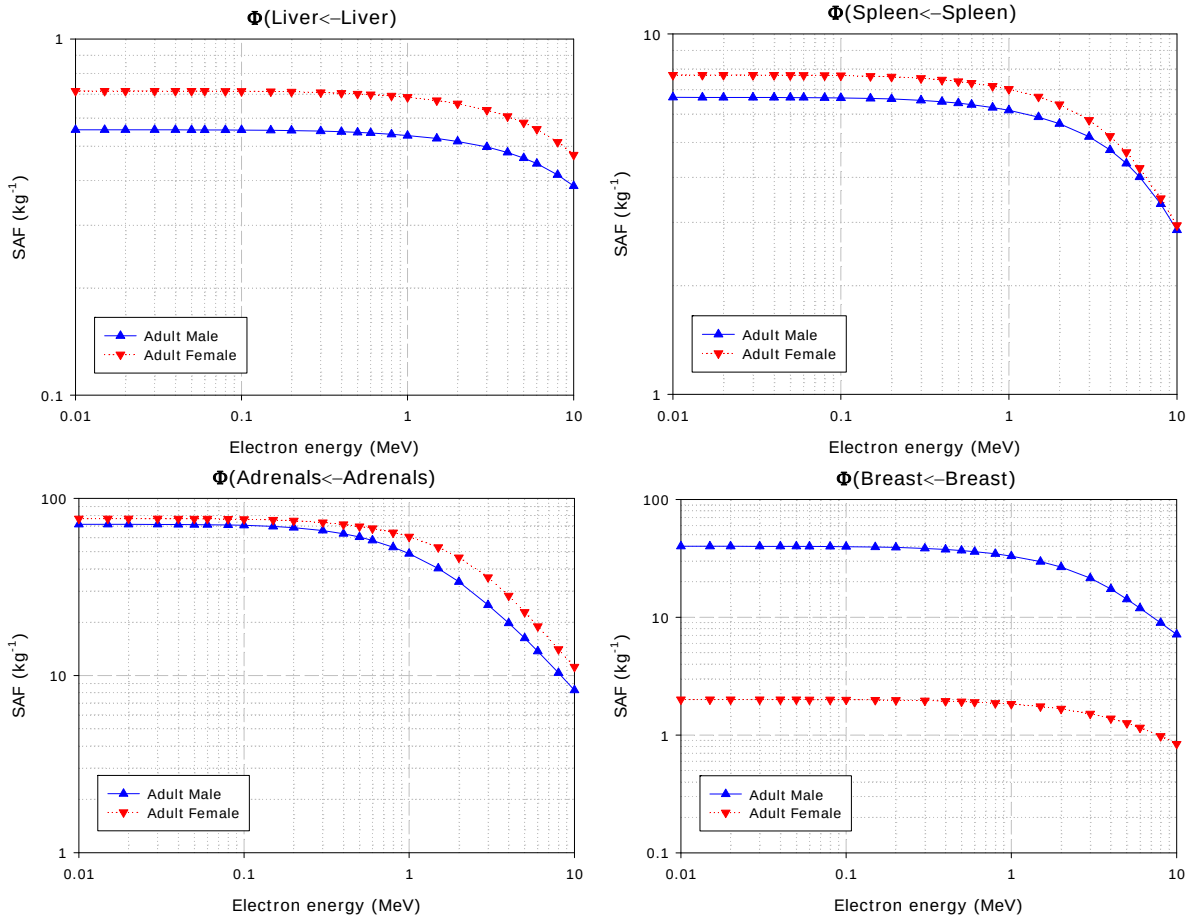

Figure 2. Specific absorbed fractions (kg^{-1}) for self-absorption of monoenergetic electrons in various source regions. Top left: liver, top right: spleen, bottom left: adrenals, bottom right: breast

In Figure 2 specific absorbed fractions for self-absorption in the source regions liver, spleen, adrenals and breast obtained by the Monte Carlo simulations are shown. As can be seen, the SAF values are constant and agree with the inverse organ mass for electron energies up to approximately between 300 keV and 1 MeV. Electrons with higher energies have an increasing ability to leave the source region, and the SAF values decrease with increasing electron energy. For larger organs, such as the liver with masses of 1.8 kg and 1.4 kg for the male and female phantom, respectively, this effect is only moderate, since many of the electrons released inside a large source region will still be absorbed in this same region, since their range is smaller than their initial distance from the surface. For small organs, such as the adrenals (with masses of 0.014 kg and 0.013 kg, respectively), the drop-off of the SAF values with increasing electron energy is much more pronounced, since even shorter electron ranges are sufficient for crossing the organ boundary.

Since inverse proportionality of the self-absorption SAFs with organ mass is obviously not established for all organs and higher electron energies, the question arises in how far the self-absorption SAFs calculated with the reference computational phantoms can be transferred to persons with differing organ masses and if simple correction factors can be applied in these cases. Since for low electron energies inverse proportionality with organ mass holds, mass correction is still intuitive and might be a straightforward correction method. This possibility was, therefore, examined further. For a selection of organs, self-absorption SAF ratios for the male and female reference computational phantoms were evaluated and compared with the respective inverse mass ratios. In Figure 3, the SAF ratios for the adrenals, brain, lungs and breast have been divided by the inverse mass ratios of these organs to show the degree by which the SAF ratios deviate from the inverse mass ratios. For comparison, the same relation is also given for the 2/3 power of the inverse mass ratios, the recommended scaling factor for photon self-absorption SAFs (Petoussi-Henss *et al* 2007, Snyder *et al* 1975).

It can be seen that for the organs with only moderate mass differences between the two phantoms also the self-absorption SAFs differ moderately and the deviations between the SAF ratios and the inverse mass ratios remain relatively small. For the adrenals, this deviation is at most 33%, for the brain the maximum deviation is 1.1%, and for the lungs it is 1.9%. Not shown in this figure are, e.g., adipose tissue, gall bladder wall, kidneys, liver, pancreas, spleen, thymus, thyroid and skin with maximum deviations between the SAF ratios and the inverse mass ratios of 13.4%, 23.2%, 2.5%, 4.8%, 15%, 10.7%, 11.8%, 1.3%, and 11.4% respectively. For all these organs, the self-absorption SAFs for one of the reference computational phantoms could be evaluated from those for the other phantom by a simple organ mass correction with only moderate errors up to between 1.1% and 33%. For the breast, the situation is different: Here the deviation of the self-absorption SAF ratios from the inverse mass ratio exceeds 40% for electron energies above 3 MeV and ranges up to a factor of 2.35 which makes a simple organ mass correction inappropriate for evaluating the SAFs for one phantom from those for the other one. In this case, correction by the 2/3 power of the inverse mass ratio is superior for electron energies above 3 MeV.

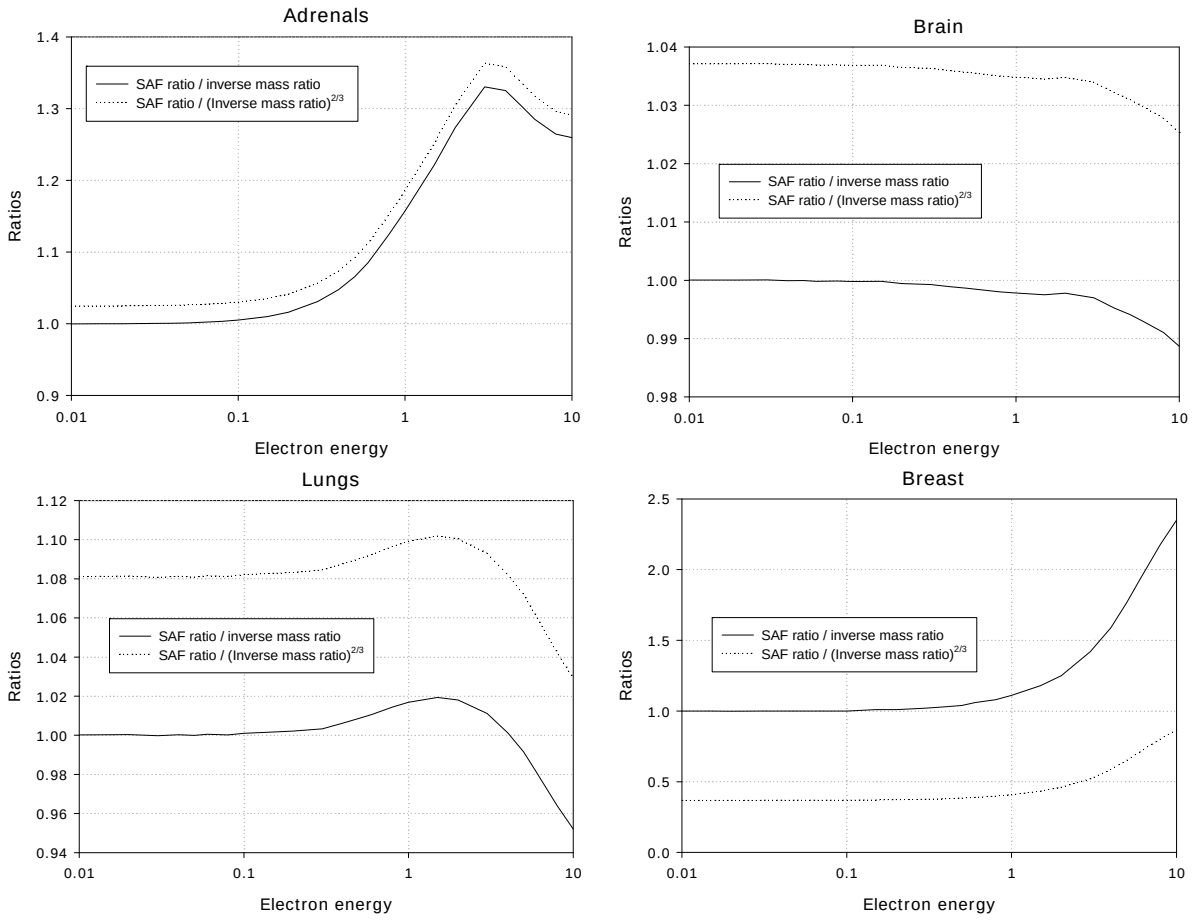

Figure 3. SAF ratio between the female and male reference computational phantom divided by the inverse organ mass ratio for adrenals (top left), brain (top right), lungs (bottom left) and breast (bottom right).

According to Ulanovsky and Pröhl (2006), self-absorption SAFs for electrons to aquatic biota of various sizes and shapes are governed by both the mass and the degree by which the body deviates from an ideal spherical shape – the so-called "non-sphericity parameter". These results have recently been confirmed by Amato *et al*. (2011). The present findings support this evidence: among the organs with moderate mass differences considered above, the deviation between the SAF ratio and the inverse mass ratio is smallest for the brain (1.1% deviation from an inverse mass ratio of 1.12), which is the least "non-spherical" among the organs considered, whereas this deviation is larger for the adrenals (33% maximum deviation from an inverse mass ratio of 1.08).

There are several organs and tissues that could not be segmented at their exact reference mass in the reference computational phantoms. Beside the fine target regions (stem cell populations) in the alimentary and respiratory tract and in the skeleton, as already mentioned above, these are the gall bladder wall, the lymphatic tissue, the adipose tissue and the skin. For the gall bladder wall, skin and adipose tissue a simple mass correction was applied to the SAFs as calculated with the reference phantoms, since for these regions the mass deviations from the reference values are only moderate and, hence, this seems acceptable according to the findings above. The entirety of the lymphatic nodes along the extrathoracic and thoracic airways is highly non-spherical and the masses of these regions in the RCP-AM and RCP-AF differ substantially from the reference values, so that a mass correction appears to be inappropriate. Therefore, separate calculations for self-absorption in these tissues were performed, for which the phantom voxel dimensions were scaled by the same factor in all three dimensions, so that the masses of LN-ET and LN-Th were in agreement with the reference masses of ICRP Publication 66 (ICRP 1994), while the non-sphericity of these

regions was the same as in the phantoms with original size. It should be noted that these separate calculations were only used for the evaluation of self-absorption SAFs in these source/target regions, not for cross-fire to or from other regions.

Table 3 lists the source/target regions whose masses in the reference computational phantoms differ from the reference values of ICRP Publication 89 and summarises the measures that have been taken to correct the self-absorption SAFs for these organs.

Table 3. Source/target regions in the reference computational phantoms for which the phantom masses differ from the reference values of ICRP Publication 89 (ICRP 2002) and measures applied to correct for these deviations

Region	Male Phantom mass (kg)	Reference mass (kg)	Female Phantom mass (kg)	Reference mass (kg)	Measure taken male	female
					Multiplication of calculated SAFs with	
AI	1.201	1.100	0.9505	0.9041	1.092	1.051
GB-wall	0.0139	0.010	0.0102	0.008	1.390	1.275
Skin	3.728	3.300	2.7215	2.300	1.130	1.183
Adipose	20.458	18.200	23.596	22.500	1.124	1.049
					Separate calculations with all voxel dimensions multiplied with	
LN-ET	0.002258	0.015	0.001335	0.012	1.880	2.079
LN-Th	0.006398	0.015	0.003864	0.012	1.329	1.459

2. *Assumption* $\Phi(r_T \leftarrow r_S) = 0$ *for organ cross-fire*

As a consequence of the assumption of equation (1) that all electrons are absorbed locally in the source region, it is equally assumed that electrons do not enter other target regions and, hence, cross-fire SAFs must be equal to zero. Since the assumption of local electron absorption has been disproved above, it can be obviously concluded that those electrons that leave the source region enter other target regions in the vicinity and result in non-zero cross-fire SAFs. Examples are shown in the following.

Cross-fire electron SAFs are shown in Figure 4 for selected source and target region combinations, together with the respective SAFs for monoenergetic photons. In most cases, where the source and target regions are distant from each other, the electron SAFs are indeed quite small. This is shown exemplarily for cross-fire from the thyroid to lungs and breast and for cross-fire from lungs to colon. In these cases, the assumption of the SAFs being equal to zero is quite acceptable for energies below a few MeV. For organ pairs that are in close vicinity, however, such as the liver and stomach wall, the cross-fire SAFs are negligible only for low electron energies; for electron energies above 1-2 MeV, they reach the same order of magnitude as those for photons and even exceed the photon SAFs for energies above 3 MeV.

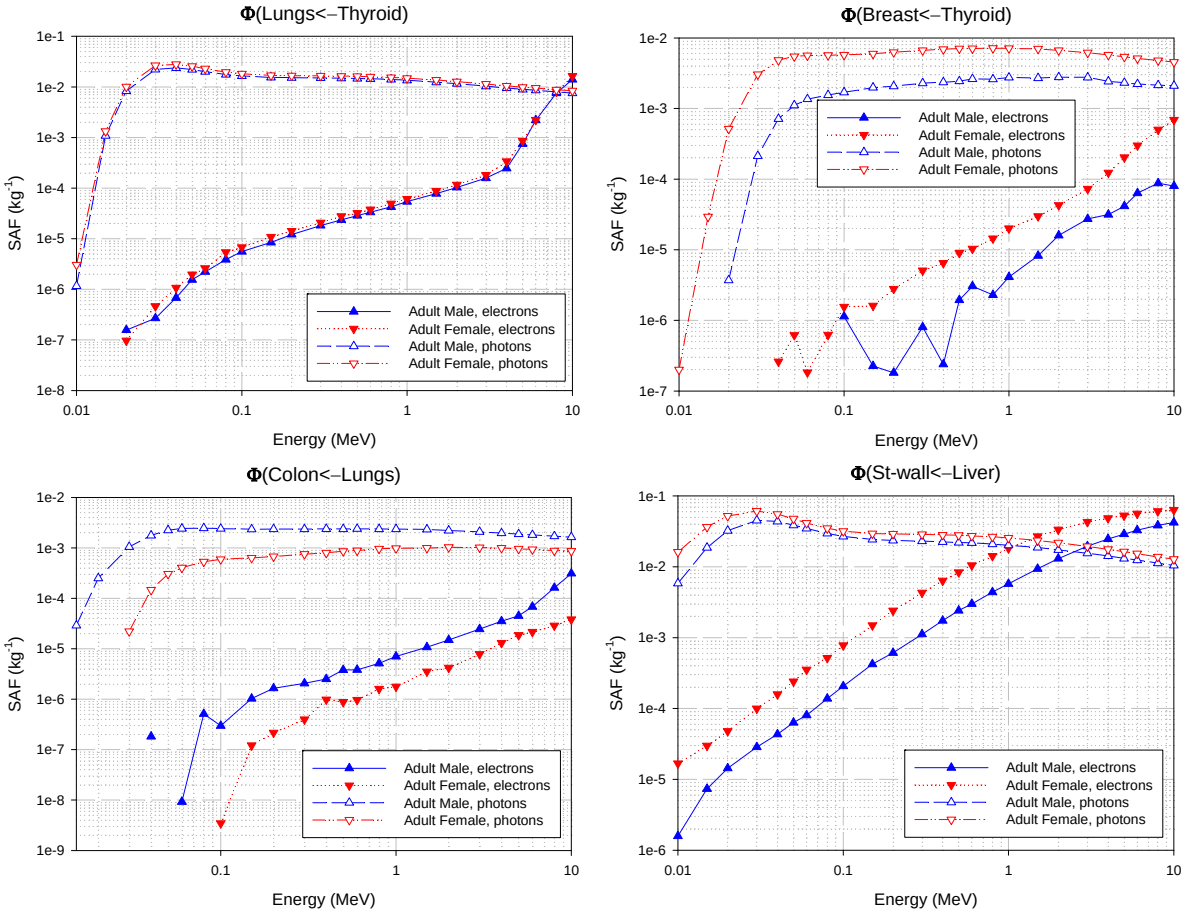

Figure 4. Cross-fire SAFs for electrons for selected source/target region pairs. Top: source thyroid, left: target lungs, right: target breast; bottom left: source lungs, target colon; bottom right: source liver, target stomach wall. For comparison, the respective SAFs for photons (ICRP 2009) are shown as well.

3. *Assumption* $\Phi(r_T \leftarrow r_S) = 0.5/M_c$ *for absorption in the wall when the source is in the contents of a walled organ*

The approximation of the dose to the wall by the dose at the surface of a half-space, or half the equilibrium dose to the contents was introduced by Snyder *et al* (1974). Since for the organs of the alimentary tract separate electron SAF values for self-irradiation of the walls and for irradiation of the walls by activity in the contents are given in ICRP Publication 100 (ICRP 2006), this approximation was retained only for the gall bladder and the urinary bladder. Figure 5 shows the electron SAFs for RCP-AM and RCP-AF for irradiation of the gall bladder and urinary bladder walls by activity in the contents, together with the values as proposed by equation (2). With a UB-cont mass of 200 g, the urinary bladder of both reference computational phantoms is modelling a relatively full bladder. Software tools for the evaluation of Specific Effective Energies, such as SEECAL (Cristy and Eckerman 1993), use rather a bladder mid-way in the void cycle, about half full. Therefore, the respective value from (2) for a urine mass of 120 g is also shown. It can be seen that for both organs the approximation of (2) results in an overestimation of the electron SAFs for all energies; for electron energies below 300 keV, the overestimation is between one and three orders of magnitude.

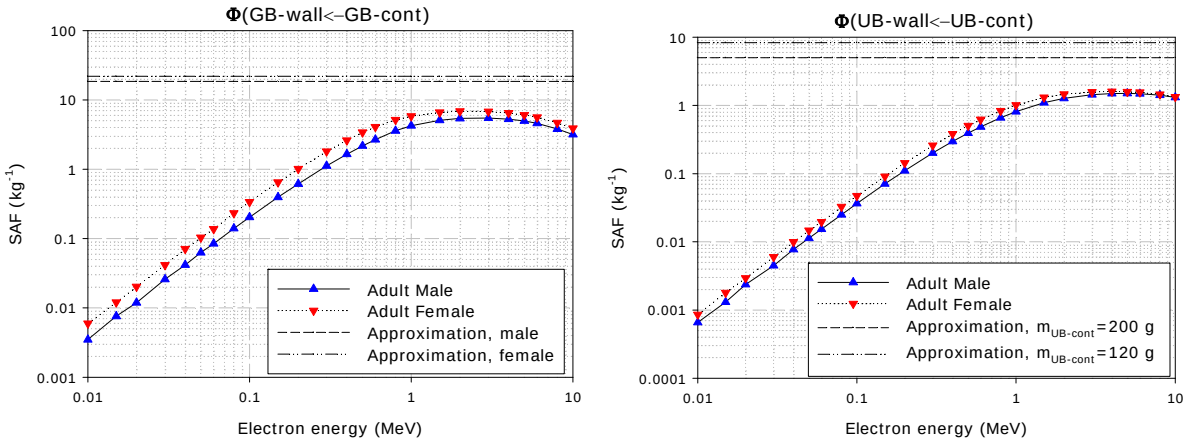

Figure 5. Electron SAFs for irradiation of the gall bladder wall (left) and the urinary bladder wall (right) from sources in the contents. For comparison, the constant values of half the equilibrium dose to the contents are given as well.

4. *Assumption* $\Phi(r_S \leftarrow r_{TB}) = 1/M_{TB}$ *for the total body as source*

The 4th assumption of (1) simply reflects the fact that for a uniform distribution of activity in the body, the fraction of activity present in a region T is exactly that region's mass fraction of the total body mass, together with the assumption of local deposition of all released electrons. In Figure 6 some examples of SAFs to lungs, adrenals, colon and skin from the total body as source region are shown. It should be noted that the total body mass to be considered in this case is that of the whole body without the contents of walled organs, i.e., 71.85 kg for the male and 58.92 kg for the female reference computational phantom. The inverse values are 0.01392 kg^{-1} and 0.01697 kg^{-1}, respectively. It can be seen that for the lungs, there is very good agreement of the SAF values with this approximation, with only a tiny drop-off at energies above 6 MeV. For the adrenals, the limited statistical accuracy of the data with coefficients of variance up to 1.1% is reflected by a slight shakiness of the curve. Nevertheless, the SAF seem to have a slight tendency to decrease with increasing energy. For the colon, the SAFs are correctly represented by the approximation of (2) only up to approximately 0.1 MeV, where they start to decrease down to approximately 80% of the approximation at 6 MeV. The reason for this effect is due to the contents of the walled organs not being included in the total body source. While the energy depositions in the colon wall at very low electron energies stem mainly from electrons that originate in the wall itself and are absorbed locally, the energy depositions of higher-energy electrons occur at increasing distance from their origin. Electrons originating in the colon wall travel both into the colon contents and into the abdominal region outside the colon, whereas electrons entering the colon wall can only stem from the abdominal region, exclusive of the colon contents. Therefore, the drop-off of the SAF values above 0.1 MeV results from the lack of electron equilibrium between the regions outside and inside the colon. Also for the skin, the SAF values are well represented by the inverse of the total body mass up to 0.1 MeV. Above this electron energy, the SAF values decrease down to approximately one half of this value at 10 MeV. The reason is similar to the situation described for the colon: electrons originating in the skin and escaping from it can either travel deeper into the body or leave the body, whereas only electrons from inside the body can enter the skin, and there are no electrons from outside that could counterbalance those lost from the body.

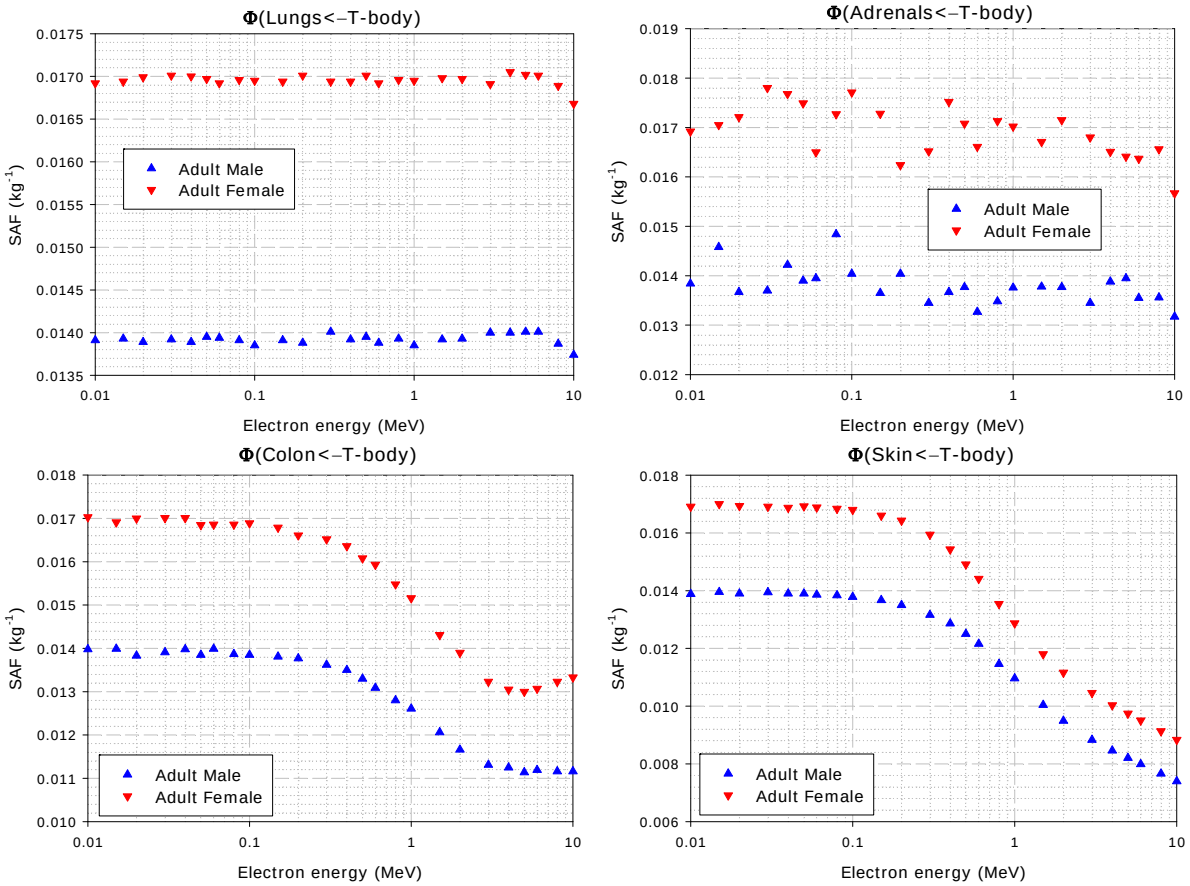

Figure 6. Electron SAFs for irradiation of selected target regions for a whole-body source. Top left: lungs, top right: adrenals, bottom left: colon, bottom right: skin.

5. *Reciprocity of cross-fire SAFs*

A further topic of interest was to examine if there is reciprocity between cross-fire SAFs for electrons, similar to the situation for photons; that means, if the following relation holds

$$\Phi(r_T \leftarrow r_S) \approx \Phi(r_S \leftarrow r_T) \quad (4)$$

and the SAFs are approximately the same when the source and target regions are exchanged. In Figure 7 selected examples are given comparing cross-fire SAFs when source and target regions are exchanged. The cases cover neighbouring (adrenals and kidneys) as well as distant organ pairs (thyroid and liver), and large mass differences between the organs, such as between adipose tissue and stomach wall.

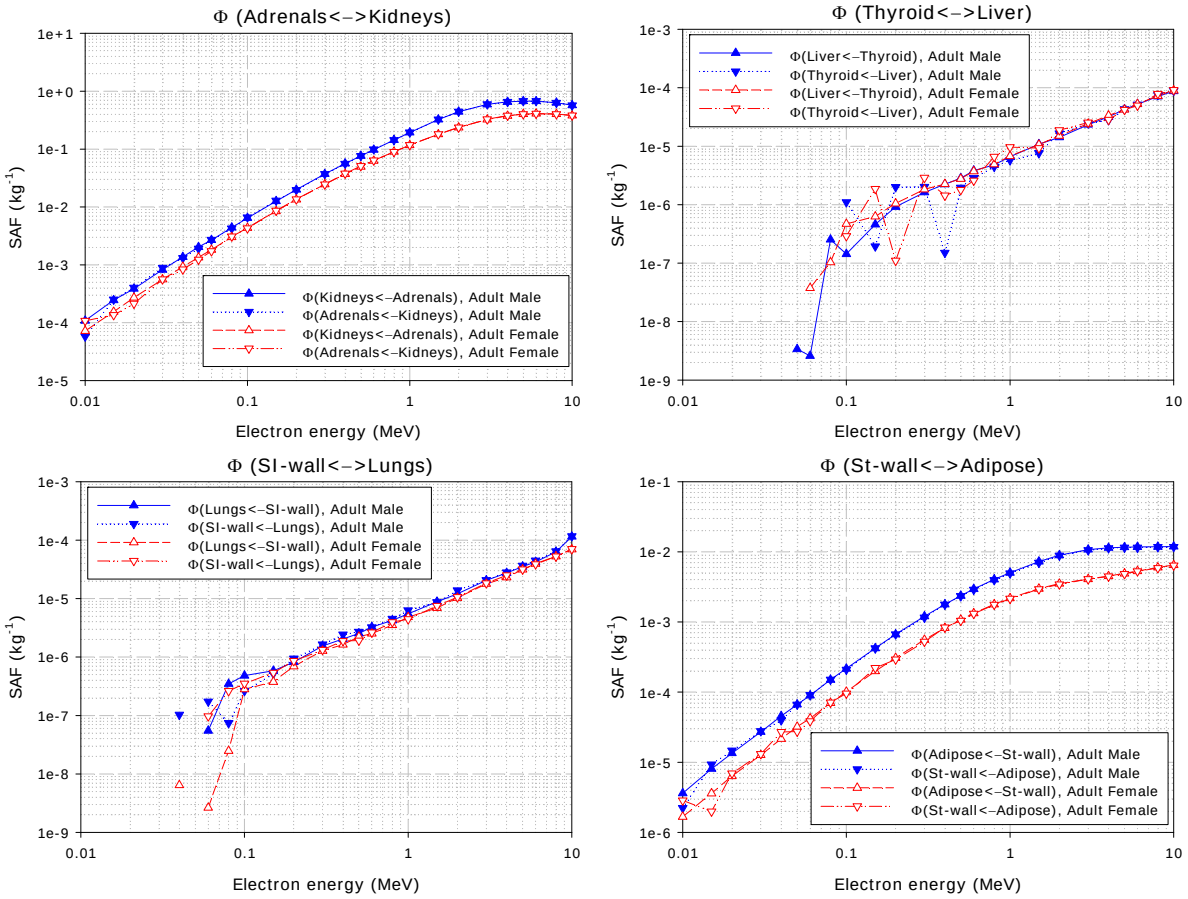

Figure 7. Examples for electron cross-fire SAFs when source and target regions are exchanged. Top left: adrenals and kidneys, top right: thyroid and liver, bottom left: small intestine wall and lungs, bottom right: stomach wall and adipose tissue.

It can be seen that in all these cases, reciprocity between source and target regions is established at least for electron energies above 0.5 MeV. In those two cases with coefficients of variance below approximately 10%, i.e., between adrenals and kidneys and between stomach wall and adipose tissue, reciprocity is approximately established in the whole energy range. The SAF differences for adrenals and kidneys as source/target organ pair are below 3.6% for electron energies above 70 keV; the SAF differences for stomach wall and adipose tissue as source/target organ pair are below 6.5% for electron energies above 80 keV. For the other two source and target organ pairs, the SAF differences are larger, but the statistical uncertainties are such that the differences are still not significant. Further examples for which reciprocity of the SAF values was examined in detail are the following organ pairs: adrenals and liver; kidneys and liver; gall bladder wall and liver; heart wall and liver; pancreas and liver; stomach wall and liver. A summary of the results of this comparison is given in Table 4. Although at low electron energies, the SAFs from source to target region may be different from those from target to source by nearly an order of magnitude, the differences were found to be moderate above energies between 60 and 600 keV, and the arithmetic mean of the differences for all energies from 10 keV to 10 MeV and both phantoms were mostly below 5%, except for thyroid and liver caused by large statistical uncertainties when thyroid is the target. From this we concluded that the reciprocity principle (Cristy 1983) does not only hold for photon but also for electron SAFs.

Table 4. Summary of the deviations of SAF values between selected organ pairs when source and target regions are exchanged. The following data are given: the maximum deviation together with the electron energy at which it occurs, the upper limit of the deviations above a certain electron energy, and the arithmetic mean of all deviations at the 25 energy points considered, for both phantoms, i.e., an arithmetic mean of up to 50 individual deviations from the reciprocity principle.

Source/target region pair		Maximum deviation	At energy	Deviations are below	For energies above	Average deviation
Region 1	Region 2	(%)	(MeV)	(%)	(MeV)	(%)
St-wall	Adipose	81	0.015	10.1	0.100	2.8
Adrenals	Kidneys	88	0.010	3.6	0.080	2.1
Adrenals	Liver	73	0.015	10.6	0.100	4.2
GB-wall	Liver	10	0.015	4.0	0.100	0.5
Ht-wall	Liver	78	0.010	9.8	0.100	5.2
Kidneys	Liver	109	0.015	5.3	0.150	4.9
Pancreas	Liver	28	0.015	11.9	0.080	0.3
St-wall	Liver	207	0.010	14.0	0.060	3.1
Thyroid	Liver	851	0.200	44.7	0.600	70.9
SI-wall	Lungs	368	0.080	19.3	0.200	0.7

From the reciprocity principle, a further important property of cross-fire SAFs can be deduced: Obviously, the SAFs do not differ much between such largely different source and target regions as, e.g., stomach wall (with a mass of 150 g and 140 g for RCP-AM and RCP-AF, respectively) and adipose tissue (with masses of 20458 g and 23596 g, respectively), when the role of source and target region is exchanged. Thus, the SAFs can be quite similar for target regions having quite different masses. Hence, in these cases the target region mass cannot be of primary significance. Equivalently, the same holds also for the source region mass. Hence, it can be concluded that the dominating principle must be the geometric relation between both regions and neither source nor target region mass. It is assumed that the reason for this behaviour is a relatively weak dose gradient within the body at larger distances from the source regions.

This opens up new possibilities for those source and target regions that could not be segmented realistically in the reference computational phantoms due to the small dimensions of these tissues and the limited (voxel) resolution of the phantoms. Due to the above conclusions, it is not important for a source or target region to have the correct mass, but it is important that all regions have an approximately anatomically realistic shape and are at their correct locations in the body. This is, however, the case also for those source and target regions in the skeleton and in the alimentary and respiratory tracts that have been excluded from the calculation of self-absorption SAFs due to the reasons discussed above. Consequently, there is no need to exclude these regions from the calculation of cross-fire SAFs as well. Therefore, electron SAFs for cross-fire between regions inside and outside the alimentary and respiratory tracts and the skeleton have been evaluated with the reference computational phantoms, and these values are included in the respective data tables. As discussed in detail above, this applies only to cross-fire SAFs, and no attempt has been made to evaluate self-absorption electron SAFs for these fine structures in the RCP-AM and RCP-AF reference computational phantoms.

Table 5. Source and target regions in the alimentary and respiratory tracts and in the skeleton, for which the SAF calculations performed with the reference computational phantoms partly cannot be used. For the source and target organ pairs where "+" is entered, SAF values have been evaluated with the RCP-AM and RCP-AF reference computational phantoms and are included in the electronic data files. Those combinations for which electron SAFs could not reasonable be evaluated on the basis of these phantoms are marked with "–". For the colon, separately evaluated regional self-absorption SAFs in the RC-wall, LC-wall and RSig-wall were combined with cross-fire SAFs from and to the other parts of the colon.

Source region	Target region												
	R-marrow Endost-BS	St-wall	Oeso-phagus	O-mucosa S-glands	SI-wall	RC-wall	LC-wall	RSig-wall	ET ET1-bas	ET ET2-bas	Bronch-bas, Bronch-sec	Bchiol-sec	All other target regions
O-cavity	+	+	+	–	+	+	+	+	+	+	+	+	+
Teeth-S	+	+	+	–	+	+	+	+	+	+	+	+	+
Oesophag-f	+	+	–	+	+	+	+	+	+	+	+	+	+
Oesophag-s													
St-cont	+	–	+	+	+	+	+	+	+	+	+	+	+
St-wall	+	–	+	+	+	+	+	+	+	+	+	+	+
SI-cont	+	+	+	+	–	+	+	+	+	+	+	+	+
SI-wall	+	+	+	+	–	+	+	+	+	+	+	+	+
SI-villi													
RC-cont	+	+	+	+	+	–	+	+	+	+	+	+	+
RC-wall	+	+	+	+	+	–	+	+	+	+	+	+	+
LC-cont	+	+	+	+	+	+	–	+	+	+	+	+	+
LC-wall	+	+	+	+	+	+	–	+	+	+	+	+	+
RSig-cont	+	+	+	+	+	+	+	–	+	+	+	+	+
RSig-wall	+	+	+	+	+	+	+	–	+	+	+	+	+
ET1-sur	+	+	+	+	+	+	+	+	–	+	+	+	+
ET2-sur	+	+	+	+	+	+	+	+	+	–	+	+	+
ET2-bnd													
ET2-seq													
Bronchi	+	+	+	+	+	+	+	+	+	+	–	+	+
Bronchi-b													
Bronchi-q													
Bronchiole	+	+	+	+	+	+	+	+	+	+	+	–	+
Brchiole-b													
Brchiole-q													
C-bone-S	–	+	+	+	+	+	+	+	+	+	+	+	+
C-bone-V													
T-bone-S	–	+	+	+	+	+	+	+	+	+	+	+	+
T-bone-V													
C-marrow	–	+	+	+	+	+	+	+	+	+	+	+	+
T-marrow	–	+	+	+	+	+	+	+	+	+	+	+	+
R-marrow	–	+	+	+	+	+	+	+	+	+	+	+	+
Y-marrow	–	+	+	+	+	+	+	+	+	+	+	+	+
All other source regions	+	+	+	+	+	+	+	+	+	+	+	+	+

6. Absorbed doses per administered activity for selected radiopharmaceuticals

In the previous sections it has been shown that the assumptions of equations (1) and (2) of local electron absorption are not always true. High-energy electrons leave the source region and may enter target regions that are not too distant. For source/target-region pairs in close vicinity and at higher electron energies, the electron SAFs can reach the same magnitude as those for photons. While corrections for electron escape from small organs and high energies are performed on the basis of self-absorption SAFs for unit-density spheres in the most widespread software for dosimetry in nuclear medicine, OLINDA/EXM, electron cross-fire to neighbouring organs is not considered (Stabin and Konijnenberg 2000, Stabin *et al* 2005). The importance of specific electron transport calculations to evaluate radiopharmaceutical S values for newborn patients has been shown by Wayson et al. (2012).

In the following, absorbed doses per administered activity for selected radiopharmaceuticals for the adult reference computational phantoms are evaluated (a) based on the above calculations where electron transport is simulated explicitly and (b) with the assumption of local electron absorption, in order to examine the implications of the above findings for realistic situations.

The following radiopharmaceuticals have been examined for this purpose:

- ^{18}F-FDG, a glucose analogue used in the investigation of myocardial and cerebral glucose metabolism,
- ^{123}I-BMIPP, an iodine-labelled free fatty acid used to study the energy metabolism of the heart and
- ^{68}Ga-EDTA, a positron-emitting substance used in PET studies of renal function.

The radionuclides ^{18}F, ^{123}I and ^{68}Ga are all beta and gamma emitters. Photon and electron energies were taken from the decay data in ICRP Publication 107 (ICRP 2008a). ^{18}F has a single photon energy at 511 keV (annihilation photons), and the beta+ energies range from 50 eV to 617 keV (mean energy 250 keV); ^{123}I has 17 photon energies with the main energy at 159 keV; the mean energy of the beta spectrum is 132 keV; the main gamma line of ^{68}Ga is at 511 keV (annihilation photon), the main beta+ line is at 836 keV and the beta energies range from 57 eV to 2.8 MeV. The photon SAFs used for these evaluations were also calculated at our department and will form the basis for the photon SAF values to be published shortly by the ICRP (ICRP in preparation). The SAF values for the individual energy lines were interpolated from the SAF calculations performed for a fixed energy grid using log–log interpolation. For the calculation of organ absorbed dose coefficients, an in-house software was used which utilises both photon and electron voxel SAFs (Petoussi-Henss *et al* 2005). The following standard formulation was used:

$$D(r_T) = \sum_{r_S} \tilde{A}(r_S) S(r_T \leftarrow r_S) + \tilde{A}(REM) \left[(M_{\mathrm{T-body}} S(r_T \leftarrow \mathrm{T-body}) - \sum_{r_S} M_{r_S} S(r_T \leftarrow r_S)) / M_{REM} \right] \quad (5)$$

with $D(r_T)$: absorbed dose in the target region, $\tilde{A}(r_S)$: time integrated or cumulated activity (equal to the total number of transformations) in the source region, $S(r_T \leftarrow r_S)$: S value (absorbed dose in target region per unit of cumulated activity in source region (mGy MBq^{-1} s^{-1})), *T-body*: total body without contents of walled organs, *M*: mass (g), *REM*: remaining tissues ($M_{REM} = M_{T\text{-}body} - \sum M_S$). The value of the expression in square brackets is the calculated S value for the remaining tissues (note that in this term the contents of walled organs are excluded from the summation over the source organs). The organ absorbed dose coefficients were evaluated using the SAFs for photons together with (a) the calculated SAFs for electrons, and (b) the currently used assumptions that electrons are locally absorbed.

Organ absorbed doses per administered activity of the above radiopharmaceuticals as calculated with the electron SAF values of this work are given in Table 6 for ^{18}F-FDG, in Table 7 for ^{123}I-BMIPP and in Table 8 for ^{68}Ga-EDTA. The deviation from these values of the respective organ dose coefficients that would be obtained when local electron absorption were assumed, is given as percentage of the values of this study. For comparison with the dose coefficients of ICRP Publication 80 (ICRP 1998) and ICRP Publication 106 (ICRP 2008b), the arithmetic mean of the values of this work for RCP-AM and RCP-AF have been evaluated (values not given in the tables), and the deviation of the ICRP published values is expressed as percentage of this arithmetic mean value.

Table 6. Organ absorbed doses per administered activity (in mGy MBq^{-1}) of the radiopharmaceutical ^{18}F-FDG for both adult reference computational phantoms, calculated with the electron SAF data of this work. Percentage deviations from these values are given for the respective organ absorbed doses as calculated with the ICRP 30 approximations. Further comparison is made with the data of ICRP Publication 106 (ICRP 2008b) by expressing the differences between the ICRP 106 values and the arithmetic mean of the values of this work for RCP-AM and RCP-AF as percentage difference to the latter. The source regions are indicated with an asterisk; the asterisk is parenthesised when the source is in the contents of a walled organ. The largest fraction by far of the time integrated activity is in the "remaining tissues" source region.

Target region		Organ absorbed dose per administered activity (mGy MBq^{-1}) calculated with the electron SAF values of this work		Percentage deviation of values as calculated with the assumption of local electron absorption		Percentage deviation of the ICRP 106 values from the values of this work
		RCP-AM	RCP-AF	RCP-AM	RCP-AF	Average
R-marrow		1.25E-02	1.45E-02	-0.16	-0.30	-18.63
Colon		1.19E-02	1.45E-02	0.71	0.65	-1.52
Lungs	*	1.89E-02	2.29E-02	0.67	0.07	-4.26
St-wall		1.23E-02	1.34E-02	0.36	0.27	-14.50
Breast		9.06E-03	1.15E-02	0.03	0.06	-14.20
Ovaries			2.14E-02		0.24	-34.54
Testes		9.64E-03		-0.27		14.09
UB-wall	(*)	5.38E-02	5.73E-02	154.11	140.88	133.92
Oesophagus		1.50E-02	1.73E-02	-1.41	-2.62	-25.78
Liver	*	2.20E-02	2.65E-02	0.25	0.27	-13.47
Thyroid		1.00E-02	1.19E-02	-0.27	-0.52	-8.75
Endost-BS		1.04E-02	1.25E-02	-0.25	-0.30	-3.80
Brain	*	3.55E-02	3.92E-02	0.44	0.44	1.73
S-glands		9.30E-03	1.18E-02	-0.02	0.07	
Skin		7.17E-03	8.55E-03	2.92	3.47	-0.72
Adrenals		1.25E-02	1.60E-02	0.12	-0.55	-15.78
ET		1.03E-02	1.25E-02	-0.42	0.22	
GB-wall		1.44E-02	1.69E-02	-1.22	-1.37	-17.08
Ht-wall	*	6.16E-02	7.89E-02	3.60	3.85	-4.64
Kidneys		1.17E-02	1.36E-02	-0.07	-0.13	34.34
Lymph		1.35E-02	1.47E-02	-1.47	-1.11	
Muscle		9.47E-03	1.15E-02	0.00	-0.03	-4.53
O-mucosa		1.01E-02	1.19E-02	-0.37	-0.49	
Pancreas		1.28E-02	1.38E-02	0.04	0.08	
Prostate		2.63E-02		-1.31		
SI-wall		1.30E-02	1.62E-02	0.43	0.21	
Spleen		1.14E-02	1.30E-02	-0.17	-0.18	
Thymus		1.18E-02	1.48E-02	-0.41	-1.26	
Uterus			3.00E-02		-0.52	

For most organs, the influence of the electron SAFs is very small and the organ dose coefficients calculated with the assumption of local electron absorption differ by less than one or two per cent from the values employing Monte Carlo calculated electron SAF values. Slightly larger deviations of 2.9%, 3.5%, 3.6% and 3.9% are observed for the skin and the heart wall. The overestimation of the skin dose is due to the large contribution of the total body source, for which the assumption of local electron absorption neglects the fact that electrons with kinetic energies above 100 keV leave the body, and thus electron equilibrium is not established (see Figure 6). The overestimation of the dose to the heart wall is probably due to the ability of electrons of higher energy to leave the source organs (for examples see Figure 2). Although the heart wall with masses of 330 g and 250 g for RCP-AM and RCP-AF, respectively, is not a small organ, its small thickness allows more electrons to escape from this source region compared to solid source regions, such as lungs, liver and brain, where the

overestimations are insignificantly small. The largest deviations of 154% and 141% for RCP-AM and RCP-AF, respectively, are seen for the urinary bladder wall. Here the assumption that the dose to the wall is half the equilibrium dose to the contents leads to pronounced overestimations (see Figure 5). The larger deviations of the organ dose coefficients of ICRP Publication 106 from the present values are mainly due to the different anatomical relations between the source and target regions of both types of phantoms used for the calculations and can be attributed to a large extent to differences in the photon SAFs (Zankl *et al* 2003).

Table 7. Organ absorbed doses per administered activity (in mGy MBq^{-1}) of the radiopharmaceutical ^{123}I-BMIPP for both adult reference computational phantoms, calculated with the electron SAF data of this work. Percentage deviations from these values are given for the respective organ absorbed doses as calculated with the ICRP 30 approximations. Further comparison is made with the data of ICRP Publication 106 (ICRP 2008b) by expressing the differences between the ICRP 106 values and the arithmetic mean of the values of this work for RCP-AM and RCP-AF as percentage of the latter. The source regions are indicated with an asterisk; the asterisk is parenthesised when the source is in the contents of a walled organ. The largest fraction by far of the time integrated activity is in the "remaining tissues" source region.

Target region		Organ absorbed dose per administered activity (mGy MBq^{-1}) calculated with the electron SAF values of this work		Percentage deviation of values as calculated with the assumption of local electron absorption		Percentage deviation of the ICRP 106 values from the values of this work
		RCP-AM	RCP-AF	RCP-AM	RCP-AF	Average
R-marrow		1.25E-02	1.50E-02	0.27	-0.09	-19.78
Colon		1.37E-02	1.52E-02	0.33	0.11	-2.80
Lungs		1.54E-02	1.81E-02	-0.26	-0.25	-22.45
St-wall		1.66E-02	1.80E-02	0.04	-0.10	-24.87
Breast		9.52E-03	1.22E-02	0.08	-0.06	-17.99
Ovaries			1.90E-02		-0.38	-26.49
Testes		1.12E-02		-0.28		-10.96
UB-wall	(*)	2.74E-02	2.79E-02	59.99	58.71	41.08
Oesophagus		1.81E-02	2.00E-02	0.19	-0.39	-31.68
Liver	*	3.91E-02	4.69E-02	0.01	-0.48	-16.28
Thyroid		1.14E-02	1.33E-02	-1.30	0.26	-11.09
Endost-BS		1.07E-02	1.30E-02	-0.38	-0.06	68.32
Brain		9.61E-03	1.13E-02	-0.02	-0.04	-8.17
S-glands		8.81E-03	1.11E-02	-0.18	-0.03	
Skin		7.77E-03	9.41E-03	0.56	0.70	-12.65
Adrenals		1.79E-02	2.33E-02	0.58	-0.68	-27.13
ET		8.96E-03	1.14E-02	0.02	-0.04	
GB-wall		2.41E-02	2.76E-02	0.07	-1.02	-26.43
Ht-wall	*	5.17E-02	6.52E-02	0.50	0.32	-9.35
Kidneys		1.61E-02	1.88E-02	-0.15	-0.11	-25.64
Lymph		1.47E-02	1.66E-02	0.11	-0.33	
Muscle		1.08E-02	1.33E-02	0.35	-0.03	-8.52
O-mucosa		9.66E-03	1.16E-02	0.12	-0.11	
Pancreas		1.86E-02	1.94E-02	-0.09	-0.14	-15.79
Prostate		1.88E-02		0.00		
SI-wall		1.44E-02	1.69E-02	0.18	0.03	-10.58
Spleen		1.40E-02	1.63E-02	0.16	-0.10	-20.75
Thymus		1.31E-02	1.65E-02	0.15	-0.43	-12.07
Uterus			2.11E-02		0.09	

Similarly to the previous comparison, the differences between calculations with and without specific electron transport simulations remain negligible, except for the urinary bladder wall, for which the simplified evaluation overestimates the doses by approximately 60%. The

differences attributed to anatomical differences of the body phantoms used for the calculations are again much more pronounced.

Table 8. Organ absorbed doses per administered activity (in mGy MBq^{-1}) of the radiopharmaceutical ^{68}Ga-EDTA for both adult reference computational phantoms, calculated with the electron SAF data of this work. Percentage deviations from these values are given for the respective organ absorbed doses as calculated with the ICRP 30 approximations. Further comparison is made with the data of ICRP Publication 80 (ICRP 1998) by expressing the differences between the ICRP 80 values and the arithmetic mean of the values of this work for RCP-AM and RCP-AF as percentage of the latter. The source regions are indicated with an asterisk; the asterisk is parenthesised when the source is in the contents of a walled organ. The largest fraction by far of the time integrated activity is in the "remaining tissues" source region.

Target region		Organ absorbed dose per administered activity (mGy MBq^{-1}) calculated with the electron SAF values of this work		Percentage deviation of values as calculated with the assumption of local electron absorption		Percentage deviation of the ICRP 80 values from the values of this work
		RCP-AM	RCP-AF	RCP-AM	RCP-AF	Average
R-marrow		1.18E-02	1.35E-02	-0.42	-1.01	-24.93
Colon		1.24E-02	1.75E-02	4.19	-2.17	-13.02
Lungs		8.85E-03	1.04E-02	0.09	0.05	-14.93
St-wall		8.55E-03	1.02E-02	7.75	7.83	-1.97
Breast		7.80E-03	9.51E-03	1.32	1.09	-13.36
Ovaries			2.87E-02		-0.23	-47.76
Testes		1.04E-02		0.11		15.31
UB-wall	(*)	2.44E-01	2.84E-01	152.11	117.67	123.36
Oesophagus		9.21E-03	1.08E-02	-0.55	0.41	-16.96
Liver		9.56E-03	1.13E-02	0.08	-0.34	-14.74
Thyroid		8.51E-03	1.02E-02	0.13	0.43	-12.18
Endost-BS		9.93E-03	1.19E-02	-0.36	-0.82	-15.62
Brain		8.09E-03	9.70E-03	-0.10	-0.01	-13.43
S-glands		7.94E-03	9.76E-03	0.08	0.11	
Skin		6.83E-03	8.10E-03	17.44	20.20	4.51
Adrenals		1.35E-02	1.42E-02	-17.02	-9.76	-32.00
ET		7.90E-03	9.91E-03	0.62	0.22	
GB-wall		8.51E-03	1.06E-02	14.41	13.24	2.52
Ht-wall		9.14E-03	1.07E-02	0.30	0.32	-12.44
Kidneys	*	4.94E-02	5.59E-02	6.52	5.76	2.53
Lymph		1.45E-02	1.49E-02	-7.68	-2.87	
Muscle		9.71E-03	1.18E-02	0.02	-0.29	-9.70
O-mucosa		8.35E-03	1.01E-02	-0.38	-0.17	
Pancreas		1.00E-02	1.23E-02	1.13	-0.54	-13.82
Prostate		4.74E-02		-18.61		
SI-wall		1.45E-02	2.01E-02	0.15	-4.65	-30.71
Spleen		9.53E-03	1.12E-02	0.01	0.13	-11.14
Thymus		8.57E-03	1.04E-02	-0.14	-0.37	-12.52
Uterus			5.00E-02		-10.96	

In contrast to ^{18}F and ^{123}I, the decay spectrum of ^{68}Ga contains also beta energies in the energy range above a few hundred keV. Hence, in this case a certain extent of the differences between calculations with and without specific electron transport simulations can be observed that can be expected from the above discussions. For the kidneys, the assumption of local electron absorption results in overestimations of the dose of 6.5% and 5.8% for RCP-AM and RCP-AF, respectively, since the high-energy betas have the ability to leave the source region and deposit a non-negligible part of their energy outside, e.g. in the adrenals, the dose of which is consequently underestimated by approximately 17% and 10% for RCP-AM and RCP-AF, respectively, if local electron absorption is assumed. Similarly, as expected from

Figure 6, the doses to superficial target regions and the walled organs of the alimentary tract from the total body source region are overestimated by up to 20%. For the female phantom, however, the overestimation of the doses to the colon and the small intestine wall from the total body source is more than compensated by the underestimation of the dose to these target regions from activity in the urinary bladder contents. Due to anatomic differences, the SAF values for the intestine target regions from the source in the urinary bladder contents are much higher for the female phantom than for the male, so that for the latter phantom the overestimation is not fully compensated. The overestimation by 152% and 118%, respectively, for the dose to the urinary bladder wall by the simplified evaluation is again quite pronounced, whereas the assumption of local electron absorption underestimates the doses to the prostate and the uterus, which are both adjacent to the urinary bladder, by 18% and 11%, respectively. Similarly to the other radiopharmaceuticals of this study, for the majority of the other organs the differences attributed to anatomical differences of the body phantoms used for the calculations are again higher than those from the different models of electron absorption.

Conclusions

The explicit Monte Carlo calculation of electron SAF values showed that high-energy electrons have the ability to leave the source organ. Consequently, the ICRP 30 approach assuming full absorption of electrons in the source organ presents an overestimation for organ self-absorption and an underestimation for organ cross-fire for electron energies above approximately 1 MeV. For neighbouring organs, such as stomach contents and liver, electron SAFs can reach the same magnitude as those for photons for kinetic energies above 1 MeV. For irradiation of the urinary bladder wall and the gall bladder wall by activity in the contents, the energy-independent values from the ICRP 30 assumption present a substantial overestimation, especially for electron energies below 1 MeV. For the total body as source region, the approximation of all electron SAFs by the inverse of the total body mass presents an overestimation for walled organs (the contents of which are excluded from the total body source) and superficial regions, such as the skin, due to lacking electron equilibrium.

Comparison of electron SAF values for a variety of region pairs showed in general approximate similarity of the values when source and target region are exchanged. This suggests that the reciprocity principle that is well-known for photons can be extended to electron SAFs as well. Hence, it can further be concluded that the principle dominating the electron SAF values is the geometric relation between the source and target regions, and neither source nor target region mass, thus making cross-fire electron SAFs mass-independent. Therefore, the cross-fire electron SAFs of the present study can be extended also to such source and target regions that have much smaller dimensions than the voxels of the reference computational phantoms and that could hence not be represented in these phantoms at their realistic resolution.

Comparing organ absorbed doses per administered activity for several radiopharmaceuticals evaluated with and without explicit electron transport calculations revealed that for most organs, the decrease in source organ self-dose and increase in organ cross-fire dose for neighbouring organs have only limited impact on the overall absorbed dose values, and the approximations of ICRP Publication 30 result in reliable dose estimates, as long as the electron energies of the decay spectra remain below a few hundred keV. The expected under- and overestimations can be observed only for radionuclides involving electron energies above several hundred keV. In contrast to most other organs, however, the dose to the urinary

bladder wall is significantly lower using the calculated electron SAFs, compared to the ICRP 30 approach, due to the large difference in SAFs, especially at electron energies below 1 MeV. For the radiopharmaceuticals considered in this work, overestimations of the dose to the urinary bladder wall between approximately 60% and 150% were found. The urinary bladder contents are an important source region for all radiopharmaceuticals and the absorbed dose to the bladder wall is often among the doses limiting the amount of activity that can be administered. Hence, this finding may prove to be important for radiopharmaceutical dosage.

Acknowledgements

This work was partially carried out within the Collaborative Project "MADEIRA" (www.Madeira-project.eu), co-funded by the European Commission through EURATOM Seventh Framework Programme (Grant Agreement FP7-212100). Furthermore, the authors express their gratitude to the Task Group DOCAL of ICRP Committee 2, especially Wesley Bolch, University of Florida, Gainesville, and Keith Eckerman, Oak Ridge National Laboratory, Oak Ridge, for fruitful discussions.

References

Amato E, Lizio D and Baldari S 2011 Absorbed fractions for electrons in ellipsoidal volumes *Phys. Med. Biol.* 56 357-65

Berger M J 1963 *Methods in Computational Physics,* ed B Alder*, et al.*: Academic, New York) pp 135-215

Chao T C and Xu X G 2001 Specific absorbed fractions from the image-based VIP-Man body model and EGS4-VLSI Monte Carlo code: internal electron emitters *Phys. Med. Biol.* 46 901-27

Cristy M 1983 Applying the reciprocal dose principle to heterogeneous phantoms: practical experience from Monte Carlo studies *Phys. Med. Biol.* 28 1289-303

Cristy M and Eckerman K F 1987a Specific absorbed fractions of energy at various ages from internal photon sources, Part I: Methods *ORNL Report* TM-8381/V1 (Oak Ridge, TN: Oak Ridge National Laboratory)

Cristy M and Eckerman K F 1987b Specific absorbed fractions of energy at various ages from internal photon sources, Part II: One-year-old *ORNL Report* TM-8381/V2 (Oak Ridge, TN: Oak Ridge National Laboratory)

Cristy M and Eckerman K F 1987c Specific absorbed fractions of energy at various ages from internal photon sources, Part III: Five-year-old *ORNL Report* TM-8381/V3 (Oak Ridge, TN: Oak Ridge National Laboratory)

Cristy M and Eckerman K F 1987d Specific absorbed fractions of energy at various ages from internal photon sources, Part IV: Ten-year-old *ORNL Report* TM-8381/V4 (Oak Ridge, TN: Oak Ridge National Laboratory)

Cristy M and Eckerman K F 1987e Specific absorbed fractions of energy at various ages from internal photon sources, Part V: Fifteen-year-old male and adult female *ORNL Report* TM-8381/V5 (Oak Ridge, TN: Oak Ridge National Laboratory)

Cristy M and Eckerman K F 1987f Specific absorbed fractions of energy at various ages from internal photon sources, Part VI: Newborn *ORNL Report* TM-8381/V6 (Oak Ridge, TN: Oak Ridge National Laboratory)

Cristy M and Eckerman K F 1987g Specific absorbed fractions of energy at various ages from internal photon sources, Part VII: Adult male *ORNL Report* TM-8381/V7 (Oak Ridge, TN: Oak Ridge National Laboratory)

Cristy M and Eckerman K F 1993 SEECAL 2.0. Program to calculate age-dependent specific effective energies *RSICC Computer Code Collection CCC-620* (Oak Ridge, TN: Oak Ridge National Laboratory)

Guo B, Xu X G and Shi C 2010 Specific absorbed fractions for internal electron emitters derived for a set of anatomically realistic reference pregnant female models *Radiat. Prot. Dosim.* 138 20-8

Hadid L, Desbrée A, Schlattl H, Franck D, Blanchardon E and Zankl M 2010 Application of the ICRP/ICRU reference computational phantoms to internal dosimetry: calculation of specific absorbed fractions of energy for photons and electrons *Phys. Med. Biol.* 55 3631-41

Hough M, Johnson P, Rajon D, Jokisch D, Lee C and Bolch W 2011 An image-based skeletal dosimetry model for the ICRP reference adult male—internal electron sources *Phys. Med. Biol.* 56 2309

ICRP 1979 Limits for intakes of radionuclides by workers. Part 1 *ICRP Publication* 30 (Oxford, UK: Pergamon Press)

ICRP 1994 Human respiratory tract model for radiological protection *ICRP Publication* 66 (Oxford, UK: Pergamon Press)

ICRP 1998 Radiation dose to patients from radiopharmaceuticals *ICRP Publication* 80 (Oxford, UK: Pergamon Press)

ICRP 2002 Basic anatomical and physiological data for use in radiological protection: reference values *ICRP Publication* 89 (Oxford, UK: Pergamon Press)

ICRP 2006 Human alimentary tract model for radiological protection *ICRP Publication* 100 (Oxford, UK: Elsevier)

ICRP 2007 The 2007 Recommendations of the International Commission on Radiological Protection *ICRP Publication* 103 (Oxford, UK: Elsevier)

ICRP 2008a Nuclear decay data for dosimetric calculations *ICRP Publication* 107 (Oxford, UK: International Commission of Radiological Protection)

ICRP 2008b Radiation dose to patients from radiopharmaceuticals *ICRP Publication* 106 (Oxford, UK: International Commission of Radiological Protection)

ICRP 2009 Adult reference computational phantoms *ICRP Publication* 110 (Oxford, UK: International Commission on Radiological Protection)

ICRP 2010 Conversion coefficients for radiological protection quantities for external radiation exposures *ICRP Publication* 116 (Oxford, UK: International Commission on Radiological Protection)

ICRP in preparation Specific absorbed fractions for internal emitters in the adult reference computational phantoms International Commission on Radiological Protection)

ICRU 1984 Stopping powers for electrons and positrons *ICRU Report* 37 (Bethesda, MD: International Commission on Radiation Units and Measurements)

ICRU 1992 Photon, electron, proton and neutron interaction data for body tissues *ICRU Report* 46 (Bethesda, MD: International Commission on Radiation Units and Measurements)

Johnson P B, Bahadori A A, Eckerman K F, Lee C and Bolch W E 2011 Response functions for computing absorbed dose to skeletal tissues from photon irradiation – an update *Phys. Med. Biol.* 56 2347–65

Jokisch D W, Rajon D A, Bahadori A A and Bolch W E 2011a An image-based skeletal model for the ICRP reference adult maleâ€"specific absorbed fractions for neutron-generated recoil protons *Phys. Med. Biol.* 56 6857

Jokisch D W, Rajon D A, Patton P W and Bolch W E 2011b Methods for the inclusion of shallow marrow and adipose tissue in pathlength-based skeletal dosimetry *Phys. Med. Biol.* 56 2699

Kawrakow I 2002 Electron impact ionization cross sections for EGSnrc *Med. Phys.* 29 1230

Kawrakow I and Bielajew A F 1998 On the Condensed History Technique for Electron Transport *Nuclear Instruments and Methods* 142B 253-80

Kawrakow I, Mainegra-Hing E, Rogers D W O, Tessier F and Walters B R B 2009 The EGSnrc code system: Monte Carlo simulation of electron and photon transport *PIRS Report* 701 (Ottawa: National Research Council of Canada (NRCC))

Kawrakow I and Rogers D W O 2003 The EGSnrc code system: Monte Carlo simulation of electron and photon transport *PIRS Report* 701 (Ottawa: National Research Council of Canada (NRCC))

Kramer R, Cassola V F, Khoury H J, Vieira J W, de Melo Lima V J and Robson Brown K 2010 FASH and MASH: female and male adult human phantoms based on polygon mesh surfaces: II. Dosimetric calculations *Phys. Med. Biol.* 55 163-89

Kramer R, Richardson R B, Cassola V F, Vieira J W, Khoury H J, De O Lira C A B and Robson Brown K 2011 Electron absorbed fractions of energy and S -values in an adult human skeleton based on μCT images of trabecular bone *Phys. Med. Biol.* 56 1803-

Loevinger R, Budinger T and Watson E 1988 MIRD primer for absorbed dose calculations (New York, NY: Society of Nuclear Medicine)

Nelson W R, Hirayama H and Rogers D W O 1985 The EGS4 code system *SLAC Report* 265 (Stanford, CA: Stanford Linear Accelerator Center)

Petoussi-Henss N, Bolch W E, Zankl M, Sgouros G and Wessels B 2007 Patient-specific scaling of reference S-values for cross-organ radionuclide S-values: what is appropriate? *Radiat. Prot. Dosim.* 127 192-6

Petoussi-Henss N, Zankl M and Nosske D 2005 Estimation of patient dose from radiopharmaceuticals using voxel models *Cancer Biotherapy and Radiopharmaceuticals* 20 103-9

Seltzer S M and Berger M J 1985 Bremsstrahlung spectra from electron interactions with screened atomic nuclei and orbital electrons *Nuclear Instruments & methods in physics research Section B* 12 95-134

Seltzer S M and Berger M J 1986 Bremsstrahlung energy spectra from electrons with kinetic energy from 1 keV to 10 GeV incident on screened nuclei and orbital electrons of neutral atoms with Z=1-100 *Atomic data and nuclear data tables* 35 345-418

Snyder W S, Ford M R, Warner G G and Watson E E 1975 "S" absorbed dose per unit cumulated activity for selected radionuclides and organs *MIRD Pamphlet* 11, Revised (New York, NY: Society of Nuclear Medicine)

Snyder W S, Ford M R, Warner G G and Watson S B 1974 A tabulation of dose equivalent per microcurie-day for source and target organs of an adult for various radionuclides *ORNL Report* TM-5000 (Oak Ridge, TN: Oak Ridge National Laboratory)

Stabin M G, Emmons M A, Segars W P and Fernald M J 2012 Realistic reference adult and paediatric phantom series for internal and external dosimetry *Radiat. Prot. Dosim.* 149 56-9

Stabin M G and Konijnenberg M W 2000 Re-Evaluation of Absorbed Fractions for Photons and Electrons in Spheres of Various Sizes *J. Nucl. Med.* 41 149-60

Stabin M G, Sparks R B and Crowe E 2005 OLINDA/EXM: The Second-Generation Personal Computer Software for Internal Dose Assessment in Nuclear Medicine *J. Nucl. Med.* 46 1023-7

Ulanovsky A and Pröhl G 2006 A practical method for assessment of dose conversion coefficients for aquatic biota *Radiat. Environ. Biophys.* 45 203-14

Wayson M, Lee C, Sgouros G, Treves S T, Frey E and Bolch W E 2012 Internal photon and electron dosimetry of the newborn patient – a hybrid computational phantom study *Phys. Med. Biol.* 57 1433

Zankl M, Becker J, Fill U, Petoussi-Henß N and Eckerman K F 2005 GSF male and female adult voxel models representing ICRP Reference Man - the present status *The Monte*

Carlo Method: Versatility Unbounded in a Dynamic Computing World (Chattanooga, TN) (La Grange Park, USA: American Nuclear Society) on CDROM

Zankl M, Petoussi-Henss N, Fill U and Regulla D 2003 The application of voxel phantoms to the internal dosimetry of radionuclides *Radiat. Prot. Dosim.* 105 539-48

Zankl M and Wittmann A 2001 The adult male voxel model "Golem" segmented from whole body CT patient data *Radiat. Environ. Biophys.* 40 153-62